

- digitized by an 8-bit analog-to-digital converter (Matrox) installed on a 486-66 PC. Initially, a reference map of the blood vessel pattern at the surface of the cortex was obtained by means of light filtered at 550 ± 40 nm (Ealing). The camera was then focused 300 μ m below the surface of the cortex. Light from a 100-W tungsten-halogen light source driven by a dc power supply (Kepeco) was passed through a 610-nm filter and used to illuminate the cortex during data collection. Frames were summed between 0.9 to 3.6 s after stimulus onset, corresponding to the time of maximum signal as determined by our previous experiments (26). Data were analyzed with the use of in-house programs written in C++ (Borland) and IDL Research Systems.
8. Square-wave luminance gratings (typical parameters for V2: spatial frequency, 0.15 cycle per degree; drift velocity, 12° per second; 64% contrast) and subjective gratings (typical spatial frequency of subjective orientation, 0.15 cycle per degree; spatial frequency of inducing lines, 0.45 cycle per degree; drift velocity, 12° per second for V2) were shown to the animal on a 17-inch monitor positioned 28.5 cm in front of it. In some experiments, the spatial frequency of subjective edges was systematically varied. Neutral gray intensity was 6.0 cd/m². All stimuli were shown binocularly. Subjective grating stimuli of four different orientations (0° , 45° , 90° , and 135°) were randomly interleaved with square-wave luminance grating stimuli and presented 80 to 100 times. Luminance-defined inducing lines, 1 to 2 pixels wide, were orthogonal to the subjective orientation for all subjective grating stimuli. Gratings were drifted normal to the subjective edge orientation and parallel to the orientation of the inducing lines in both directions separately. Eye position and area central of both eyes were checked at the start of imaging by use of a reverse ophthalmoscope to project an image of the retinal vasculature onto the screen.
 9. Orientation maps obtained with luminance gratings composed of thin lines (of the same width as the subjective grating inducing lines) were identical to orientation maps obtained with thicker bars (Fig. 2C) and relatively independent of grating spatial frequency.
 10. We compared orientation strengths (magnitude of the orientation vector) for those pixels in V2 (Fig. 2, C and D) that had similar orientation preferences for luminance and subjective gratings (within $\pm 22.5^\circ$ orientation difference). The mean orientation strength for luminance gratings (4.56×10^{-3} units) was threefold higher than the mean orientation strength for subjective gratings (1.31×10^{-3} units) for these pixels.
 11. We vectorially summed the responses of each pixel to all orientations of luminance and subjective gratings separately, obtained the pixel's resultant orientation preferences for both, and derived the difference between the two values.
 12. Single-unit experiments were carried out in 12 cats. Single units were recorded with parylene-insulated tungsten microelectrodes. Responses were conventionally amplified, displayed, and stored. Stimulus conditions were the same as in the imaging studies.
 13. Receptive field properties of a subset of V2 cells whose luminance and subjective orientation preferences differed by $\pm 45^\circ$ or less (17 cells) were studied in detail. Most of these cells (13 cells) were complex; four cells were simple. Only 2 of the cells were end-stopped; the remainder (15 cells) were non-end-stopped. Twenty-four cells whose locations were identified were encountered at a variety of depths (160 to 1800 μ m); 11 cells were encountered in the superficial layers and 13 cells in the deep layers.
 14. We correlated the responses of single neurons ($n = 7$) to luminance and subjective gratings with the optically imaged maps. Each of the regions in the orientation difference map—in which orientation preferences for luminance and subjective orientations are similar, orthogonal, or in-between—contained neurons with matching responses.
 15. J. A. Movshon, I. D. Thompson, D. J. Tolhurst, *J. Physiol.* **283**, 101 (1978); K. Albus, *Exp. Brain Res.* **24**, 159 (1975).
 16. We compared orientation strengths for those pixels in V1 (Fig. 3C) that had similar orientation preferences for luminance and subjective gratings (within $\pm 22.5^\circ$ orientation difference). The mean orientation strength for subjective gratings (1.00×10^{-3} units) was slightly higher than the mean orientation strength for luminance gratings (0.87×10^{-3} units) for these pixels. Thus, the response to subjective gratings in V1 was stronger for subjective gratings than for luminance gratings for this subset of pixels, although they occupied a small portion of V1.
 17. Receptive field properties of a subset of V1 cells whose luminance and subjective orientation preferences differed by $\pm 45^\circ$ or less were studied in detail. Three cells were complex; one was a simple cell. Two cells were end-stopped, four cells were non-end-stopped. Six cells whose locations were identified were encountered at depths ranging from 300 to 1200 μ m from the surface.
 18. Responses to subjective gratings cannot be explained by responses to line terminations. We have shown that cells that share the same orientation preference for luminance and subjective gratings may respond optimally to a grating composed of a grid of dots (line ends) with the same parameters (spatial frequency, temporal frequency) as the subjective grating but of an entirely different orientation. Some cells that are tuned to the same orientation of luminance and subjective gratings as well as the dot grid show a sharper tuning, or a higher response, or both, to a subjective grating than to a dot grid. A response to Fourier energy alone cannot explain why the response of a cell to an intermediate subjective orientation is higher than the response at 90° orientation difference (orientation of the inducing lines in the subjective grating), because the energy along these orientations is less than the energy along the inducing-line orientation. Moreover, most such cells respond optimally to a single intermediate orientation, despite the presence of equal Fourier energy in the stimulus along both the optimal orientation and its orthogonally oriented counterpart.
 19. V2 and V1 in cats are anatomically distinct [R. Otsuka and R. Hassler, *Arch. Psychiatr. Nervenkr.* **203**, 212 (1962); D. J. Price, *Exp. Brain Res.* **58**, 125 (1985); G. H. Kageyama and M. Wong-Riley, *J. Comp. Neurol.* **243**, 182 (1986); B. R. Payne, *Vis. Neurosci.* **6**, 445 (1990); A. L. Humphrey, M. Sur, D. J. Uhlich, S. M. Sherman, *J. Comp. Neurol.* **233**, 190 (1985)]. To physiologically assess the boundary between V1 and V2, we used luminance gratings with different parameters: a grating of high spatial frequency (0.5 cycle per degree) and low drift velocity (4° per second), which V1 neurons prefer, and a grating of low spatial frequency (0.15 cycle per degree) and high drift velocity (12° per second), which V2 neurons prefer [(21)]. By distinguishing the portion of the optically imaged region that responded preferentially to the slower drift rate, higher spatial frequency stimulus (V1) compared to the higher drift rate, lower spatial frequency stimulus (V2), we could locate the V1/V2 boundary accurately. The physiological border coincided with the anatomical border between areas 17 and 18 as demonstrated by marker lesions and histology.
 20. D. H. Hubel and T. N. Wiesel, *J. Physiol. (London)* **165**, 559 (1963); *ibid.* **195**, 215 (1968); T. Bonhoeffer and A. Grinvald, *J. Neurosci.* **13**, 4157 (1993).
 21. T. Bonhoeffer, D.-S. Kim, D. Maloney, D. Shoham, A. Grinvald, *Eur. J. Neurosci.* **7**, 1973 (1995).
 22. C. Redies, J. M. Crook, O. D. Creutzfeldt, *Exp. Brain Res.* **61**, 469 (1986).
 23. See also A. F. Rossi, C. D. Rittenhouse, M. A. Paradiso, *Science* **273**, 1104 (1996); V. A. Lamme, *J. Neurosci.* **15**, 1605 (1995); D. A. Leopold and N. K. Logothetis, *Nature* **379**, 549 (1996).
 24. V1 and V2 in cats differ in their thalamic inputs as well: V1 receives input from X and Y cells located in the A-laminae of the lateral geniculate nucleus, whereas V2 receives inputs from Y cells alone [reviewed in S. M. Sherman and P. D. Spear, *Physiol. Rev.* **62**, 738 (1982)].
 25. R. L. Gregory, *Nature* **238**, 51 (1972); *ibid.* **199**, 678 (1963); I. Rock and R. Anson, *Perception* **8**, 665 (1979).
 26. S. C. Rao, L. J. Toth, B. R. Sheth, M. Sur, *Soc. Neurosci. Abstr.* **20**, 836 (1994); L. J. Toth, S. C. Rao, D.-S. Kim, D. Somers, M. Sur, *Proc. Natl. Acad. Sci. U.S.A.* **93**, 9869 (1996).
 27. S. Nelson, L. J. Toth, B. Sheth, M. Sur *Science* **265**, 774 (1994).
 28. We thank D.-S. Kim and L. Toth for assistance and E. Adelson, B. Anderson, and P. Sinha for critical reading of the manuscript. Supported by NIH grant EY07023. J.S. was supported by a fellowship from the Fogarty International Center of the NIH.

18 September 1996; accepted 28 October 1996

Requirement of CDC42 for *Salmonella*-Induced Cytoskeletal and Nuclear Responses

Li-Mei Chen, Silke Hobbie, Jorge E. Galán*

The bacterial pathogen *Salmonella typhimurium* triggers host cell signaling pathways that lead to cytoskeletal and nuclear responses required for pathogenesis. Here, the role of the small guanosine triphosphate (GTP)-binding protein CDC42Hs in these responses was examined. Expression of a dominant interfering mutant of CDC42 (CDC42HsN17) prevented *S. typhimurium*-induced cytoskeletal reorganization and subsequent macropinocytosis and bacterial internalization into host cells. Cells expressing constitutively active CDC42 (CDC42HsV12) internalized an *S. typhimurium* mutant unable to trigger host cell responses. Furthermore, expression of CDC42HsN17 prevented *S. typhimurium*-induced JNK kinase activation. These results indicate that CDC42 is required for bacterial invasion and induction of nuclear responses in host cells.

Interaction of the bacterial pathogen *Salmonella typhimurium* with host cells activates a bacterially encoded protein secre-

tion system that directs the export and, in some cases, the translocation into the host cell of several bacterial proteins (1). These proteins, in turn, trigger signal transduction pathways that lead to a variety of cellular responses.

Among these responses is an extensive reorganization of the actin cytoskeleton, re-

Department of Molecular Genetics and Microbiology, School of Medicine, State University of New York at Stony Brook, Stony Brook, NY, 11794-5222, USA.

*To whom correspondence should be addressed.

sulting in morphological changes that resemble the membrane ruffles induced by growth factors, hormones, and activated oncogenes (2). These cytoskeletal rearrangements are accompanied by macropinocytosis (3) and ultimately result in bacterial internalization into the cell. The abil-

ity of *Salmonella* to enter nonphagocytic cells is essential to pathogenesis as it allows the bacteria to breach the intestinal wall or to gain access to the intracellular environment where the host defense mechanisms can be more effectively evaded.

Previous studies have established that *Salmonella* can induce complex signaling pathways in cultured epithelial cells (4, 5). Although the understanding of these signaling events is incomplete, it is clear that the bacteria are similar to other well-characterized agonists in eliciting both cytoskeletal reorganization and induction of gene expression.

A group of low molecular weight GTP-binding proteins (CDC42, Rac, Rho) have been shown to coordinate signaling cascades that produce both morphological and nuclear responses to a variety of extracellular signals. In these cascades, in which one guanosine triphosphatase regulates the action of the next, CDC42 controls the formation of filopodia, Rac controls the subsequent formation of lamellipodia and membrane ruffling, and Rho controls the formation of stress fibers and

focal adhesions (6). We examined whether these small GTP-binding proteins contribute to the *Salmonella*-induced cellular responses. Mutants of CDC42Hs were expressed in COS-1 cells using a selection system (7) in which the cells expressing the different CDC42Hs proteins could be identified by the coupled expression of the green fluorescent protein (GFP). We transfected COS-1 cells with plasmids encoding various CDC42Hs mutants, infected the cells with wild-type *S. typhimurium*, and then looked for macropinosomes resulting from bacterially induced membrane ruffling (8) (Fig. 1, A and B). Alternatively, we fixed and treated infected cells with rhodamine-labeled phalloidin, which stains polymerized actin and therefore can reveal cytoskeletal changes (9) (Fig. 2, A and B), or we quantified bacterial internalization (10).

Expression of a dominant-negative mutant of CDC42Hs (CDC42HsN17) abrogated the cytoskeletal rearrangements (Fig. 2, B and C) and the formation of macropinosomes (Fig. 1) induced by *S. typhimurium* infection and prevented bacterial internalization into trans-

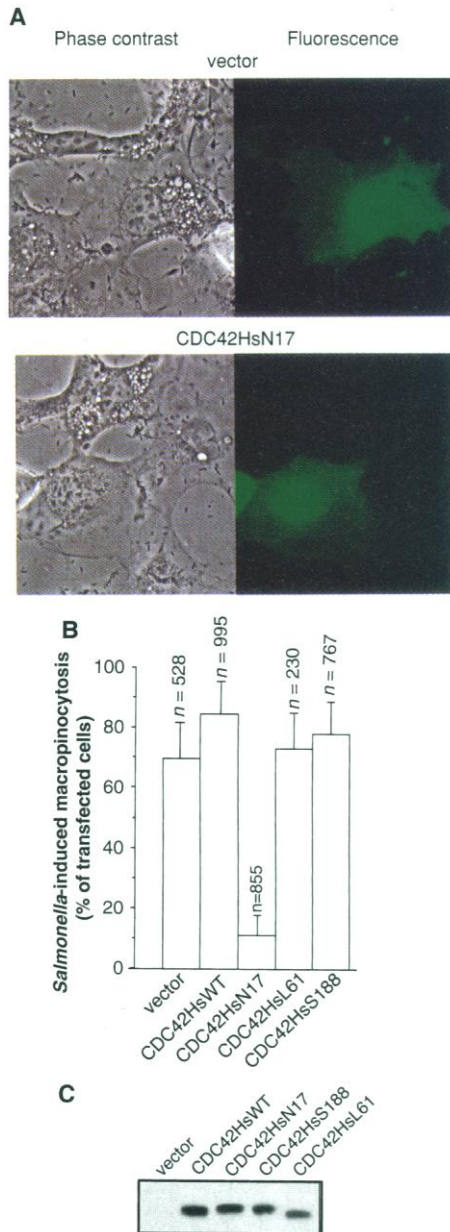


Fig. 1. Requirement of CDC42 for *Salmonella*-induced macropinocytosis. COS-1 cells were transfected with vectors coding for CDC42Hs mutants and GFP. (A) Transfected cells were infected with wild-type strain SL1344 (13) for 1 hour and examined by phase and fluorescence microscopy. (B) Quantitation of transfected cells undergoing macropinocytosis as a consequence of infection. The *n* values are the number of cells examined and represent a combination of at least five experiments. (C) Expression levels of the different CDC42 mutants in the transfected cells, as determined by immunoblot analysis.

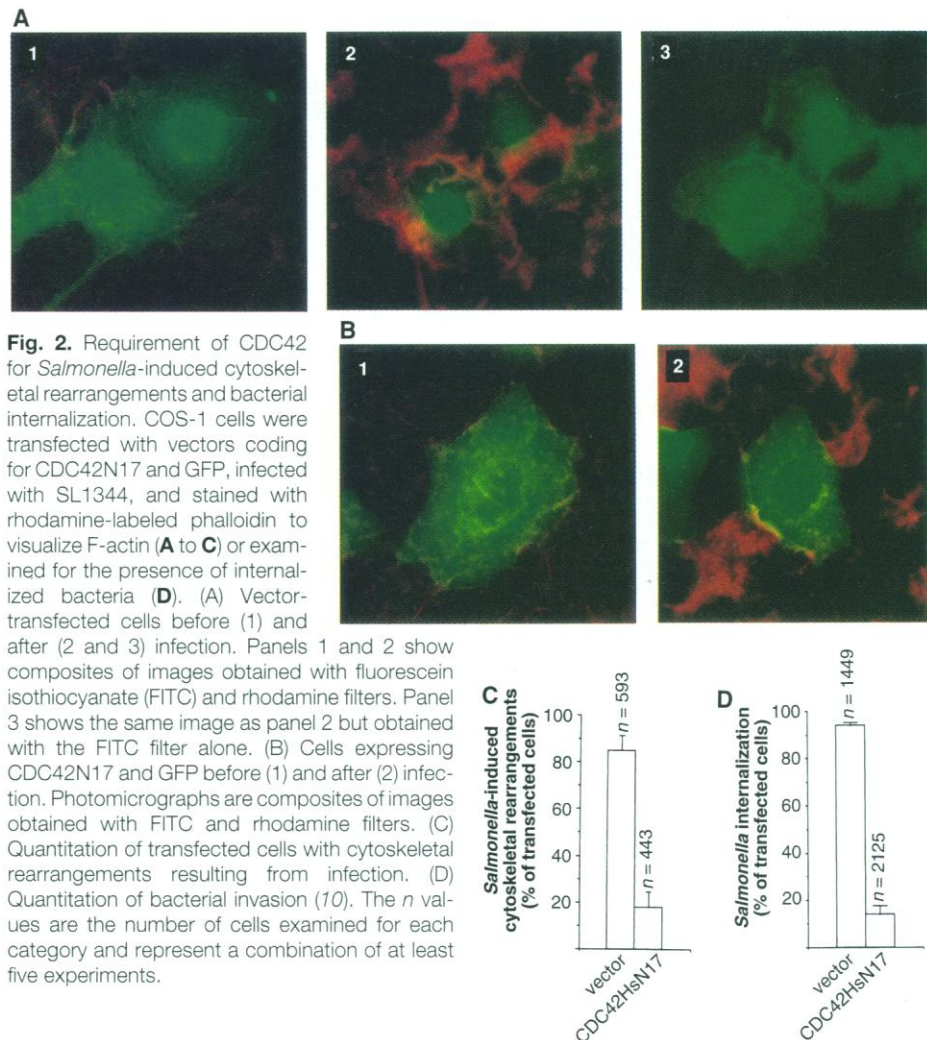


Fig. 2. Requirement of CDC42 for *Salmonella*-induced cytoskeletal rearrangements and bacterial internalization. COS-1 cells were transfected with vectors coding for CDC42HsN17 and GFP, infected with SL1344, and stained with rhodamine-labeled phalloidin to visualize F-actin (A to C) or examined for the presence of internalized bacteria (D). (A) Vector-transfected cells before (1) and after (2 and 3) infection. Panels 1 and 2 show composites of images obtained with fluorescein isothiocyanate (FITC) and rhodamine filters. Panel 3 shows the same image as panel 2 but obtained with the FITC filter alone. (B) Cells expressing CDC42HsN17 and GFP before (1) and after (2) infection. Photomicrographs are composites of images obtained with FITC and rhodamine filters. (C) Quantitation of transfected cells with cytoskeletal rearrangements resulting from infection. (D) Quantitation of bacterial invasion (10). The *n* values are the number of cells examined for each category and represent a combination of at least five experiments.

fecting cells (Fig. 2D). A small number of cells expressing CDC42HsN17 responded to infection but these cells had few macropinosomes, minor cytoskeletal rearrangements, and few internalized bacteria (less than three bacteria per cell). In contrast, expression of wild-type CDC42Hs, a prenylation-defective form (CDC42HsS188), a constitutively active form (CDC42HsL61), or GFP alone had no effect on the infection-induced cytoskeletal rearrangements and macropinocytosis (Figs. 1 and 2, A to C) and bacterial internalization (Fig. 2D). Similar results were obtained with transfected HeLa cells (11).

To test whether expression of a consti-

tutively active form of CDC42Hs confers on the cell the ability to internalize an invasion-defective mutant of *S. typhimurium*, we infected Rat-1 cells stably expressing CDC42HsV12 (12) with the noninvasive strain SB136. This strain carries a nonpolar mutation in the *invA* gene, which encodes an essential component of the invasion-associated type III protein secretion system, and therefore cannot initiate host cell signaling (13). SB136 was internalized by Rat-1 CDC42HsV12 stable transfectants but not by the control Rat-1 cells stably transfected with the vector alone (Fig. 3), indicating that activation of CDC42Hs can

rescue the invasion phenotype of the *invA* mutant. Similar results were obtained with COS-1 cells transiently expressing the constitutively active mutant CDC42L61 (11).

We next investigated whether Rac1 plays a role in the *Salmonella*-induced cytoskeletal rearrangements and bacterial internalization. COS-1 cells were transfected with an expression vector coding for Rac1 mutants (7), infected with wild-type *S. typhimurium*, and examined for macropinosomes (8), cytoskeletal changes (9), and bacterial internalization (10). Expression of a dominant interfering mutant of Rac1 (Rac1N17) modestly inhibited the bacterially induced changes, but to a much lesser extent than did CDC42HsN17 (Fig. 4). In contrast, expression of wild-type Rac1, a constitutively active form (Rac1V12), or the vector alone had no effect on bacterial internalization, cytoskeletal rearrangements, or macropinocytosis. A previous study indicated that Rac1 is not required for *Salmonella*-induced cytoskeletal rearrangements in Swiss 3T3 cells (14). This discrepancy may be due to the fact that we examined a larger number of cells, perhaps allowing detection of more subtle effects.

We have shown that *S. typhimurium* activates several transcription factors that are involved in the production of pro-inflammatory cytokines such as interleukin 8, and that these nuclear responses require activation of the MAP kinases JNK and p38 (15). It has been reported that constitutively active CDC42 leads to the activation of the JNK and p38 MAP kinases (16). We therefore tested the possibility that CDC42 is required for *Salmonella*-induced activation of JNK (17). Expression of a dominant interfering mutant of CDC42 (CDC42HsN17) prevented bacterially induced JNK activation (Fig. 5), suggesting that CDC42 is required for these nuclear responses.

The mechanisms by which CDC42 is engaged in the cellular responses to infection are not known. The strict dependence of the responses on the bacterial Type III protein secretion system suggests that translocation of a bacterial effector protein (proteins) into the host cell may stimulate the signaling pathways leading to CDC42 activation. Previous work implicating arachidonic acid metabolites in *Salmonella*-induced cytoskeletal changes (5) and Rho family function (18) raises the possibility that this cellular signaling pathway may be important.

Our results indicate that CDC42 induces cytoskeletal rearrangements independently of Rac. Although membrane ruffling has been associated more frequently with Rac activity, the relative importance of the different G proteins in modulating cytoskeletal rearrangements may largely depend on the agonist and cell type (19). Potential

Fig. 3. Rescue of an invasion-defective *S. typhimurium* mutant by expression of constitutively active CDC42HsV12. Rat-1 cells stably transfected with a CDC42HsV12-coding plasmid or the empty vector were grown on 24-well plates to ~80% confluency and infected with either wild-type SL1344 or the invasion-defective isogenic mutant SB136 (13) at a multiplicity of infection (MOI) of 10. The percentage of internalized bacteria was determined by the gentamicin resistance assay (13). For each cell line, the percentage of SL1344 internalized was taken as 100% (in different experiments the actual internalization values for SL1344 ranged from 10 to 30% of the inoculum). The values represent the mean \pm SD of triplicate samples. The difference between the SL1344 and SB136 internalization values in all cells was statistically significant ($P = <0.001$).

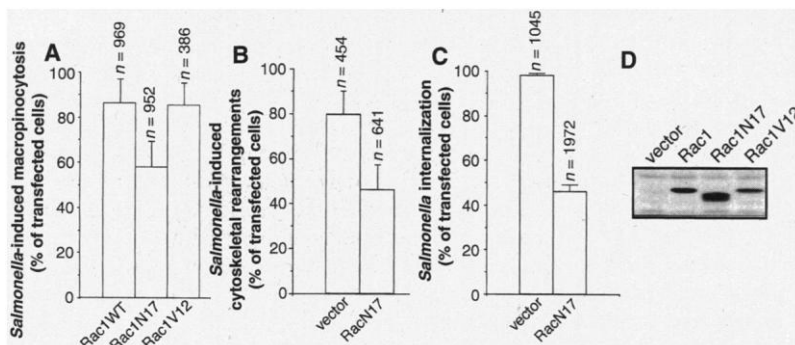
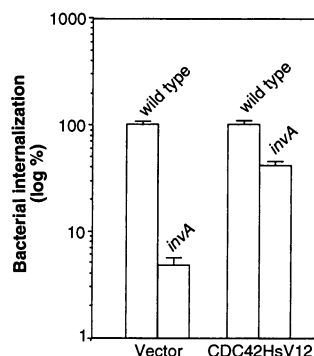
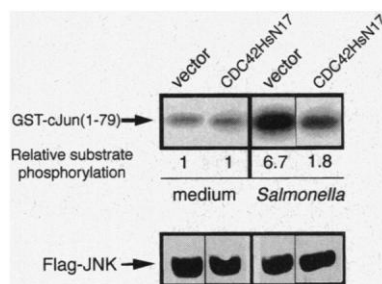


Fig. 4. Role of Rac-1 in *Salmonella*-induced cytoskeletal rearrangements, macropinocytosis, and bacterial internalization. COS-1 cells were transfected with vectors coding for Rac1 mutants and GFP and then infected with SL1344. Quantitation of transfected cells undergoing macropinocytosis (A) or cytoskeletal rearrangements (B) as a consequence of infection. (C) Quantitation of bacterial internalization. The *n* values are the number of cells examined for each category and represent a combination of at least five experiments. (D) Expression levels of the different Rac1 mutants in the transfected cells were compared by immunoblot analysis.

Fig. 5. Requirement of CDC42 for *Salmonella*-induced JNK activation. COS-1 cells were transfected with a vector coding for a FLAG epitope-tagged Jnk-1 plus either pcDNA3-CDC42HsN17 or pcDNA3. Cells were then treated with DMEM alone or infected with wild-type SL1344 in DMEM for 30 min and Jnk-1 activity was measured in an immune complex kinase assay (17). Substrate phosphorylation was quantitated by means of a PhosphorImager and relative values are shown below each lane. Similar results were obtained in at least four experiments. Expression levels of FLAG epitope-tagged Jnk-1 in the different cell lysates were compared by immunoblot analysis.



targets of CDC42 that may largely play a role in these responses include a group of protein kinases with homology to the yeast Ste20 protein (PAK kinases), the Wiskett-Aldrich syndrome protein (WASP), and phosphatidylinositol-3-kinase (PI3-kinase) (20). PI3-kinase is unlikely to play a role in *S. typhimurium*-induced signaling, however, as wortmannin, a potent inhibitor of PI3-kinase, has no effect on the *S. typhimurium*-induced cell responses (11).

REFERENCES AND NOTES

- J. E. Galán, *Curr. Topics Microbiol. Immunol.* **209**, 43 (1995); J. E. Galán, *Mol. Microbiol.* **20**, 263 (1996).
- A. Takeuchi, *Am. J. Pathol.* **50**, 109 (1967); B. B. Finlay and S. Falkow, *J. Infect. Dis.* **162**, 1096 (1990); C. Ginocchio, J. Pace, J. E. Galán, *Proc. Natl. Acad. Sci. U.S.A.* **89**, 5976 (1992); C. L. Francis, T. A. Ryan, B. D. Jones, S. J. Smith, S. Falkow, *Nature* **364**, 639 (1993).
- F. Garcia-del Portillo and B. B. Finlay, *Infect. Immun.* **62**, 4641 (1994).
- J. E. Galán, *Trends Cell Biol.* **4**, 196 (1994); J. E. Galán, J. Pace, M. J. Hayman, *Nature* **357**, 588 (1992); S. Ruschkowski, I. Rosenshine, B. B. Finlay, *FEMS Microbiol. Lett.* **74**, 121 (1992).
- J. Pace, M. J. Hayman, J. E. Galán, *Cell* **72**, 505 (1993).
- J. Chant and L. Stowers, *ibid.* **81**, 1 (1995); A. B. Vojtek and J. A. Cooper, *ibid.* **82**, 527 (1995); S. H. Zigmund, *Curr. Opin. Cell Biol.* **8**, 66 (1996); C. D. Nobes and A. Hall, *Cell* **81**, 53 (1995).
- This system consists of an SV40 early gene promoter, which drives the expression of wild-type and mutant CDC42Hs and Rac1; this first cistron is followed by the internal ribosomal entry site of encephalomyocarditis virus [S. K. Jang, M. V. Davies, R. J. Kaufman, E. Wimmer, *J. Virol.* **63**, 1651 (1989)] and the gene for a mutant form of GFP with increased fluorescence properties (GFPs65T) [R. Heim, A. B. Cubitt, R. Y. Tsien, *Nature* **373**, 663 (1995)]. The two genes are transcribed as a single dicistronic mRNA and therefore both proteins are synthesized independently but in a coupled manner. The backbone of the expression vector was from pSG5 (Stratagene). The sources of the different forms of CDC42Hs and Rac1 were as follows: CDC42HsWT, CDC42HsN17, CDC42HsS188, and CDC42HsL61 were obtained as Bam HI-Pvu II fragments of pGEX-2TKCDC42, pGEX-2TKCDC42N17, pZlneoCDC42S188, and pGEX-2TKCDC42L61, respectively [S. Bagrodia, B. Dérjard, R. J. Davis, R. A. Cerione, *J. Biol. Chem.* **270**, 27995 (1995)]; Rac1WT and Rac1V12 were obtained as 800 bp Eco RI fragments from pEX/Rac1 and pEX/Rac1Val12, respectively; and Rac1N17 was obtained by PCR from pGEX2TRac1 [A. J. Ridley, H. F. Paterson, C. L. Johnston, D. Diekmann, A. Hall, *Cell* **70**, 401 (1992)].
- COS-1 cells were grown on glass cover slips in Dulbecco's modified Eagle's medium (DMEM) supplemented with 5% fetal bovine serum (FBS) to 70% confluency and transfected with the plasmid vectors. Transfected cells were infected at an MOI of 50 for 1 hour at 37°C with wild-type *S. typhimurium* strain SL1344 that had been grown under conditions that stimulate the Type III protein secretion system [L. M. Chen, K. Kaniga, J. E. Galán, *Mol. Microbiol.* **21**, 1101 (1996)]. Cells were usually infected 24 to 36 hours after transfection, when GFP could be visualized. Infected cells maintained at 37°C were examined on a Nikon Diaphot 300 inverted microscope.
- Transfected cells grown on glass cover slips were infected with strain SL1344 for 20 min at 37°C at an MOI of 50. Cells were washed, fixed, stained with rhodamine-labeled phalloidin, and examined under a fluorescence microscope.
- Bacterial invasion was measured as in J. P. van Putten, J. F. L. Weel, and H. U. C. Grassmé [*Methods Enzymol.* **236**, 420 (1994)] with minor modifica-

tions. Each cell invaded by *Salmonella* had an average of 31 ± 14 internalized bacteria.

- L. M. Chen and J. E. Galán, unpublished data.
- A. Minden, A. Lin, F. X. Claret, A. Abo, M. Karin, *Cell* **81**, 1147 (1995).
- J. E. Galán, C. Ginocchio, P. Costeas, *J. Bacteriol.* **17**, 4338 (1992).
- B. D. Jones, H. F. Paterson, A. Hall, S. Falkow, *Proc. Natl. Acad. Sci. U.S.A.* **90**, 10390 (1993).
- S. Hobbie, L. M. Chen, R. J. Davis, J. E. Galán, unpublished data.
- C. S. Hill, J. Wynne, R. Treisman, *Cell* **81**, 1159 (1995); O. A. Coso *et al.*, *ibid.*, p. 1137.
- COS-1 cells grown in 6-cm culture dishes were transfected with 1 µg of pcDNA3-FLAG-Jnk-1, which encodes a FLAG epitope-tagged Jnk-1, and 2 µg of either pcDNA3CDC42HsN17 or the vector pcDNA3. After 48, cells were mock-infected or infected with strain SL1344 for 30 min at an MOI of 20 in DMEM. The JNK kinase activity in cell lysates was determined as described previously [S. Bagrodia, B. Dérjard, R. J. Davis, R. A. Cerione, *J. Biol.*

- Chem.* **270**, 27995 (1995)].
- M. P. Peppelenbosch *et al.*, *Cell* **81**, 849 (1995); M. P. Peppelenbosch, L. G. J. Tertoolen, W. J. Hage, S. W. de Last, *ibid.* **74**, 565 (1993); M. H. Tsai, C. L. Yu, D. W. Stacey, *Science* **250**, 962 (1990); J. W. Han, F. McCormick, I. G. Macara, *ibid.* **252**, 576 (1991); T.-H. Chuan, B. P. Bohl, G. M. Bokoch, *J. Biol. Chem.* **268**, 26206 (1993).
- T. Nishiyama *et al.*, *Mol. Cell. Biol.* **14**, 2447 (1994).
- E. Manser, T. Leung, H. Saliuddin, Z. Zhao, L. Lim, *Nature* **367**, 40 (1994); G. A. Martin, G. Bollag, F. McCormick, A. Abo, *EMBO J.* **14**, 77 (1995); M. Symons *et al.*, *Cell* **84**, 723 (1996); Y. Zheng, S. Bagrodia, R. A. Cerione, *J. Biol. Chem.* **269**, 18727 (1994).
- We thank A. Abo, R. Cerione, R. Davis, and A. Hall for plasmids and cell lines, J. Lipsick for useful discussion, and D. Bar-Sagi for critical review of this manuscript. Supported by NIH grant GM52543 to J.E.G., who is an investigator of the American Heart Association.

26 July 1996; accepted 16 October 1996

TECHNICAL COMMENTS

Consequences of Retinal Color Coding for Cortical Color Decoding

Dennis M. Dacey *et al.* in their report (1) and Richard H. Masland in his Perspective (2) draw attention to important details in the encoding of color in the retina of macaque monkeys and humans. The centers of red-green opponent retinal ganglion cells can be driven by a single cone, but the cone specificity of the surrounds is in question. Dacey *et al.* state that horizontal cells that subserve red-green opponent cells are contacted by both L- and M-cones, a finding with implications for receptive field formation (1), retinal coding (1, 2), and cortical decoding (2). While Dacey *et al.* may well be correct that surrounds are shaped by post-horizontal cell processes, I question whether mixed cone surrounds pose insurmountable problems for retinal color coding or cortical color decoding. The color signals of units with mixed cone surrounds are less complicated if the spatial properties of the units are taken into account using the Ingling-Martinez identity (3)—a rigorous statement of the co-coding hypothesis discussed by Masland. Let x be the weight of a P cell-L-cone center and y and z be the weights of M- and L-cones driving the surround. The Ingling-Martinez identity that describes this P cell is

$$xLC - (yM + zL)S = 0.5[(x + z)L + yM][C - S] + 0.5[(x - z)L - yM][C + S] \quad (1)$$

where C and S are center and surround spatial weighting or modulation transfer functions. In this equation, the first term

represents the bandpass spatial response to achromatic stimuli and the second term, the lowpass spatial response to chromatic stimuli. If $z = 0$, then the surround is pure, and the cone weighting of the achromatic and chromatic responses differ only in polarity. The effect of mixed cone surrounds is to give the achromatic and chromatic responses different cone weightings (4). This is the case psychophysically—for the CIE standard observer, the achromatic response is approximately 5L:3M, while the red-green color response is 2L:3M. Reconciling these different weights using pure surrounds has motivated several models (5). Mixed surrounds can yield this result directly [that is, if $(x, y, z) = (3.5, 3.0, \text{and } 1.5)$] and is roughly what would be expected (6) for random surrounds constructed on an L-cone rich-retina (such as that posited to underlie the standard observer's luminosity function).

Do mixed cone surrounds pose difficulties for cortical color/luminance decoding? Recent models of achromatic/chromatic demultiplexing rely on spatial filtering operations that are based on the spatial properties of the center/surround combinations in Eq. 1, but are robust with respect to surround cone ratios (4, 7–9). Filtering models have no problem accounting for the major red-green cell classes in cytochrome oxidase blobs; type II cells, $\frac{3}{4}$ double-opponent cells, and double-opponent cells can be created from filtering operations on parvo cells (8). Similar models account for extraction of achromatic information (4, 7, 9). These filtering operations do not always create a